

Nusselt Number Scaling in an Inclined Differentially Heated Square Cavity

S. W. Armfield¹, N. Williamson¹, Wenxian Lin² and M. P. Kirkpatrick¹

¹School of Aerospace, Mechanical and Mechatronic Engineering
The University of Sydney, Sydney, NSW, 2006, Australia

²College of Science, Technology and Engineering
James Cook University, Townsville, QLD 4811, Australia

Abstract

The flow structure and heat transfer in inclined two-dimensional differentially heated square cavities is investigated via numerical simulation. It is shown that the basic flow structure is changed when the cavity is inclined such that the heated wall is below the cooled wall, with attached jet/plumes forming adjacent to the adiabatic walls, rather than diffuse intrusions as for the non-inclined cavity. At a specific angle of inclination, the flow undergoes a bifurcation so that the fully developed flow is unsteady and single mode, with a further increase in inclination leading to multi-modal and then broad banded chaotic flow. The Nusselt number is obtained and plotted against the inclination angle to determine the effect of inclination on the total cavity heat transfer.

Introduction

The differentially heated square cavity, with heated and cooled opposing vertical walls, and adiabatic upper and lower boundaries, has been widely studied, providing a canonical representation of a large range of buoyancy driven flows. The flow consists of natural convection boundary layers forming on the heated/cooled walls, entraining fluid from, and discharging to, diffuse intrusions in the stratified interior. The overall flow acts to transport heat from the heated to the cooled wall, with the details of the flow depending on the temperature differential across the cavity, typically characterised by a Rayleigh (or Grashof) number, and by the Prandtl number of the fluid [4, 6, 7, 8, 11, 13]. Inclined natural convection cavity flow has received less attention, although a number of studies have investigated the effect of inclination angle on flow structure and bulk heat transfer [5, 10, 14].

In the present study the flow structure, bifurcation and transition, and total heat transfer of inclined natural convection cavity flow is investigated in detail via numerical simulations. As the cavity is inclined, so that the heated wall is below the cooled wall, the structure of the flow changes with the boundary layers formed on the heated and cooled sides discharging into attached jet/plumes adjacent to the adiabatic boundaries. This structure allows travelling waves to circulate continuously around the cavity, providing a feedback mechanism to augment the convective instability of the natural convection boundary layers, leading to an absolute instability of the total flow, with associated bifurcation, at a specific inclination angle. The total heat transfer, characterised by the average Nusselt number on the heated wall, plotted against the inclination angle, shows a complex relationship, with the Nusselt number initially increasing, before exhibiting an overall decline as would be expected.

Numerical Method

The flow and temperature fields are obtained by solving the Navier–Stokes equations expressed in two dimensional incompressible form with the Oberbeck–Boussinesq approximation for buoyancy, together with the temperature transport equation,

which are as follows,

$$u_t + uu_x + vv_y = -p_x + \frac{Pr}{Ra^{1/2}}(u_{xx} + u_{yy}) + Pr \sin \theta T, \quad (1)$$

$$v_t + uv_x + vv_y = -p_y + \frac{Pr}{Ra^{1/2}}(v_{xx} + v_{yy}) + Pr \cos \theta T, \quad (2)$$

$$u_x + v_y = 0, \quad (3)$$

$$T_t + uT_x + vT_y = \frac{1}{Ra^{1/2}}(T_{xx} + T_{yy}). \quad (4)$$

u and v are the velocity components in the x and y directions respectively, with x the direction normal to the heated wall and y the direction parallel to the heated wall, t is the time, T the temperature and p the pressure. Quantities are non-dimensionalised based on a length scale H , the length of the sides in the square cavity, temperature difference ΔT , half the temperature difference between the heated and cooled cavity sides, and characteristic velocity $U = (g\beta\Delta TH)^{1/2}/Pr^{1/2}$, with β , κ and ν the coefficient of thermal expansion, thermal diffusivity and kinematic viscosity respectively, and g the acceleration due to gravity. The control parameters are the Rayleigh number $Ra = (g\beta\Delta TH^3)/(\nu\kappa)$ and the Prandtl number, $Pr = \nu/\kappa$. θ is the angle of inclination, that is the degree of rotation in an anti-clockwise sense from the standard differentially heated cavity with vertical side-walls.

The equations are solved in the square domain $0 \leq x \leq 1.0, 0 \leq y \leq 1.0$, with the velocity set to zero on all boundaries. The temperature is set to 1.0 on the $x = 0$ boundary and -1.0 on the $x = 1$ boundary, with the other two boundaries adiabatic.

A second-order fractional step finite-volume Navier–Stokes solver defined on a non-staggered rectangular grid is used. Time integration is accomplished using an Adams–Bashforth scheme for the nonlinear terms and Crank–Nicolson for the viscous and diffusion terms. All spatial terms are discretised using centred second-order differences. Continuity is enforced and pressure obtained using a pressure correction equation. The basic code has been widely used for the simulation of natural convection cavity flow [1, 2, 3, 9, 12].

The domain is discretised with a stretched rectangular grid to allow full resolution of the small scale near wall features. The standard grid has minimum grid spacings in each direction of $\Delta x = \Delta y = 0.001$, adjacent to the boundaries, with a maximum stretching factor of 1.013 moving away from the boundaries, giving a maximum grid spacing of $\Delta x = \Delta y = 0.00256$ in the interior of the cavity. The total number of cells is 445×445 . A time-step of $\Delta t = 0.00125$ is used with the standard grid. Time step and grid dependency tests have been carried out with additional solutions obtained with half the grid size, stretching rate and time step, giving a total mesh of 919×919 cells, and one third the grid size, stretching rate and time step, giving a total

mesh of 1331×1331 cells. Point values of temperature and velocity, time averaged for the unsteady flows, were observed to vary by less than 1% over these three grids. For the unsteady flows the frequency of the single mode flow was also observed to vary by less than 1% over the three grids.

Results

All results have been obtained at Rayleigh number $Ra = 1 \times 10^8$ and Prandtl number $Pr = 7.0$, with a range of inclination angles. Figure 1 contains the fully developed stream function and temperature contours, respectively, at inclination angle $\theta = 0^\circ$, which is the standard non-inclined differentially heated square cavity flow. Natural convection boundary layers have formed adjacent to the heated (left side) and cooled (right side) boundaries, rising on the heated side and falling on the cooled side. These boundary layers discharge heated and cooled fluid into diffuse intrusions adjacent to the upper and lower adiabatic boundaries, which travel across the cavity to be entrained by the far side natural convection boundary layer. The temperature contours show the relatively narrow rising and falling natural convection boundary layers, with the interior fluid fully stratified. This flow is steady at full development.

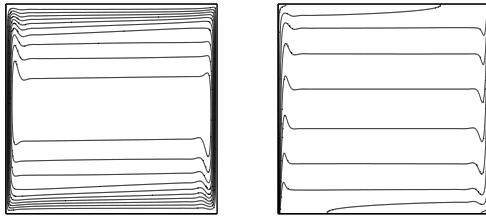


Figure 1: Stream function (left) and temperature (right) contours for $\theta = 0^\circ$.

The $\theta = 18^\circ$ results, in figure 2, clearly show the effect of the inclination angle on the flow. Natural convection boundary layers have again developed adjacent to the heated left side and cooled right side walls, but the buoyancy of the discharged fluid, combined with the inclination of the adiabatic upper and lower boundaries, means that the boundary layers now discharge into attached jet/plumes adjacent to the adiabatic boundaries. The attached jet/plumes are narrower and have a higher velocity than the diffuse intrusions observed in the $\theta = 0^\circ$ flow. The attached jet/plume flow is entrained by the far side boundary layers. The temperature contours again show the relatively narrow rising and falling natural convection boundary layers, and show that the interior of the cavity is again stratified. The $\theta = 18^\circ$ flow is also steady at full development.

Figure 3 contains the temperature and stream function contours for $\theta = 54^\circ$. In this case the fully developed flow is unsteady with a complex and irregular structure. The stream function contours show a general cavity scale circulation with much thicker boundary layers than those observed in the lower inclination angle cases. The temperature contours show relatively thin thermal boundary layers on the heated and cooled walls, but now with plumes forming and being shed into the cavity interior. The temperature in the interior of the cavity no longer displays the regular stratification that was characteristic of the lower inclination angles, indicating that the fluid is now well mixed.

Time series of the temperature at location $x = 0.004$, $y = 0.5$, that is at the half height location and immediately interior to the heated wall, are shown in figure 4 for inclination angle

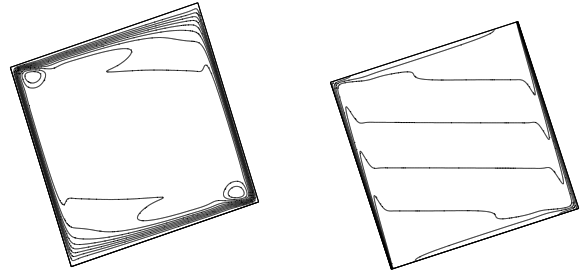


Figure 2: Stream function (left) and temperature (right) contours for $\theta = 18^\circ$.

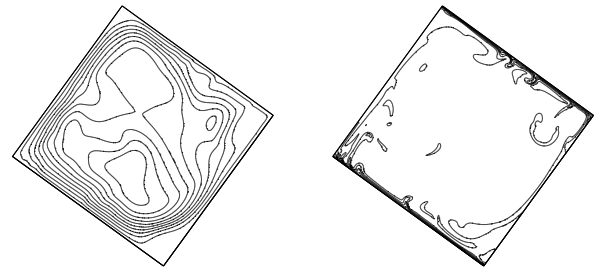


Figure 3: Stream function (left) and temperature (right) contours for $\theta = 54^\circ$.

$\theta = 37.35^\circ$. The figure shows the start-up temperature time series in the main graph, together with the fully developed longer time scale time series in the two insets. At full development the time series is displaying sustained single mode oscillatory behaviour. As noted above the flows at lower inclination angles were steady at full development, with $\theta = 36.9^\circ$ the largest inclination angle tested that is steady at full development (not shown). It is therefore apparent that a critical value of θ for transition to fully developed unsteady flow must lie between inclination angles $\theta = 36.9^\circ$ and $\theta = 37.35^\circ$.

The average Nusselt number, Nu , on the hot wall is plotted against the inclination angle in figure 5, where Nu is obtained as the integral of the negative of the normal temperature gradient over the heated wall. The Nusselt number is seen to initially increase with inclination angle up to a peak at $\theta \sim 15^\circ$. With further increase in the inclination angle Nu reduces until $\theta \sim 45^\circ$, where it shows an abrupt increase, from $Nu = 70.3$ at $\theta \sim 45^\circ$ to $Nu = 72$ at $\theta \sim 49^\circ$. Nu then reduces until a third peak occurs, with Nu increasing over $\theta \sim 65^\circ$ to $\theta \sim 67^\circ$. The lowest value of the Nusselt number is obtained at the inclination angle $\theta = 90^\circ$, when the heated and cooled walls are horizontal.

As the cavity is inclined the heat transfer mechanism varies from pure natural convection boundary layer flow, at $\theta = 0^\circ$ to pure Rayleigh Benard convection, $\theta = 90^\circ$. As the cavity is inclined, the buoyancy driving force for the natural convection boundary layers will reduce, as seen in equation (2), where the buoyancy term varies with $\cos(\theta)$. The overall reduction in Nu observed, from figure 5, is associated with this $\cos(\theta)$ reduction in the driving force for the natural convection boundary layers. Based on the known $Nu \sim Ra^{1/4}$ scaling for the non-inclined cavity; [13], the $\cos(\theta)$ variation in the buoyancy force would

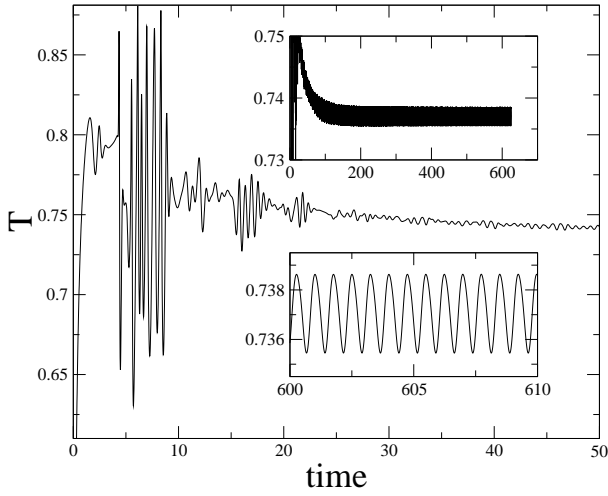


Figure 4: Time series of temperature adjacent to the heated wall for $\theta = 37.35^\circ$

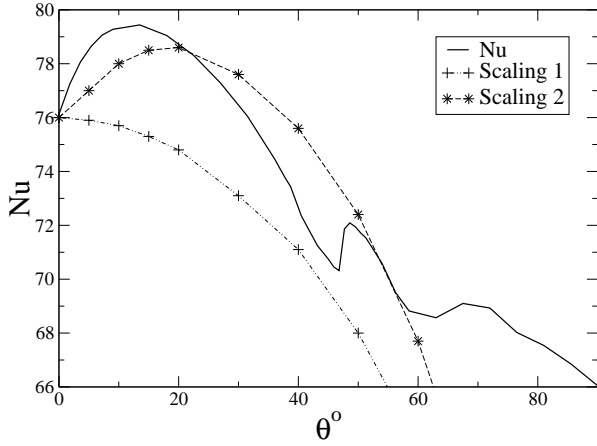


Figure 5: Nusselt number variation

be expected to lead to a scaling for the Nusselt number of,

$$Nu \sim \cos(\theta)^{1/4}.$$

This scaling is plotted as *Scaling 1* in figure 5, and is seen to capture the overall reduction in Nusselt number, but does not capture the initial increase, the two subsequent peaks, or the reduced rate of decrease as θ approaches 90° .

The sudden increase in Nu at $\theta \sim 45^\circ$ is associated with the transition of the natural convection boundary layers to fully chaotic and broad-banded unsteady flow, subsequent to the initial single mode transition described above. The increase at $\theta \sim 67^\circ$ is most likely associated with the onset of the Rayleigh Benard convection. Additionally the reduced rate of decrease as θ approaches 90° is a result of the Rayleigh Benard convection, without which the Nusselt number would be equal to 0.0 at $\theta = 90^\circ$, as for the $\cos(\theta)$ scaling.

The initial increase in the Nusselt number, up to the peak at $\theta \sim 15^\circ$, is believed to be a result of the interaction between the natural convection boundary layers and the stratification. As can be seen in figure 1, the interior of the cavity is stratified with the temperature varying from approximately the cold wall temperature at the bottom boundary to the hot wall temperature at the top boundary. As a result the temperature difference across

the boundary layer adjacent to the heated wall will reduce from a maximum value at its lower end, to a lesser value at its upper end, and the converse for the cooled wall. In the inclined cavity the interior is still stratified, as seen in figure 2, with the variation now extending over the vertical distance from the lower left corner of the cavity to the upper right corner. This means that the temperature variation across the boundary layer adjacent to the heated wall is increased, as it is effectively located in a lower, that is cooler, part of the stratification, and similarly for the cooled wall. By assuming that the temperature stratification is linear in the vertical direction, it is possible to develop a scaling approximation for this increase in boundary layer temperature variation with inclination angle. Combining it with the scaling for the variation in buoyancy forcing, given above, gives a further modified scaling for the Nusselt number,

$$Nu \sim \left[\left(1 - \frac{1}{2(\sin(\theta) + \cos(\theta))} \right) \cos(\theta) \right]^{1/4}.$$

This scaling is plotted as *Scaling 2* in figure 5. As can be seen this modified scaling provides a good representation of the initial increase in the Nusselt number, and subsequent reduction. It does not predict the peak at $\theta \sim 49^\circ$, or the subsequent peak at $\theta \sim 67^\circ$ and increasing influence of the Rayleigh Benard as the inclination angle reduces further.

Conclusions

Two-dimensional numerical solutions have been obtained for natural convection flow in inclined square cavities with differentially heated and cooled opposing walls, with the other walls adiabatic. With the heated wall on the left and the cooled wall on the right the cavity is inclined in an anti-clockwise direction so that the heated wall is then below the cooled wall. All results were obtained at Rayleigh number $Ra = 1 \times 10^8$ and Prandtl number $Pr = 7.0$.

The inclined cavity, even at small angles of inclination, is seen to have a significantly different flow structure to that of the non-inclined cavity. Referring to the flow adjacent to the heated wall only, the standard, non-inclined, cavity, has a heated natural convection boundary layer that entrains fluid over most of its lower half and discharges into a diffuse intrusion over most of its upper half. The fluid in the diffuse intrusion travels horizontally across the cavity to be entrained by the far wall boundary layer. In the inclined cavity the boundary layer entrains fluid over a smaller region of its lower half, and now discharges into an attached wall jet/plume, immediately beneath the adiabatic upper boundary. The discharged fluid travels across the cavity as an attached jet/plume, to be entrained by the boundary layer on the far wall. The temperature field of the inclined cavities for the smaller inclination angles is similar to that of the standard, non-inclined, cavity, with the interior of the cavity fully stratified and narrow thermal boundary layers adjacent to the heated and cooled walls.

At a critical angle of inclination the inclined cavity flow undergoes a bifurcation to a single mode unsteady flow. This unsteady flow is comprised of a series of waves circulating continuously around the periphery of the cavity, and travelling in the same direction as the flow, that is up the heated wall, from left to right across the cavity adjacent to the upper adiabatic wall, and down the cooled wall, from right to left across the cavity adjacent to the lower adiabatic wall. The transition to unsteady flow is a result of both the natural convection boundary layers and the attached jet/plumes being able to sustain travelling waves. Although the attached jet/plumes are stable, with the travelling waves decaying as they transit across the cavity, at a sufficient inclination angle the decay in the plumes is balanced by the am-

plification in the natural convection boundary layers leading to the observed transition.

As the inclination is increased past the critical angle the flow transits to multi-modal unsteady flow and finally to a broad-banded and chaotic regime. At the higher inclination angles Rayleigh Benard effects dominate, with plumes being generated on the heated and cooled boundaries penetrating the interior of the cavity. These plumes carry their local momentum with them leading to a cavity scale flow and fully mixed interior.

The average Nusselt number on the heated wall is also seen to vary with inclination angle. As the cavity is inclined the Nusselt number initially increases, peaking at an inclination angle of $\theta \sim 15^\circ$, before reducing with further inclination. Two subsequent peaks are observed in the Nusselt number as the cavity is further inclined, at $\theta \sim 49^\circ$, and $\theta \sim 67^\circ$. The overall decrease in Nusselt number is a result of the reduced buoyancy forcing in the flow direction on the heated and cooled walls, however the initial increase is believed to be a result of the interaction of the boundary layers and the stratification of the fluid within the cavity, which produces an increase in the local temperature variation across the boundary layers for small angles of inclination. A Nusselt number scaling, including this effect, has been shown to provide a good representation of this behaviour. The subsequent peaks are believed to be associated with the transition to broad-banded and chaotic unsteady flow in the boundary layers, and to the initiation of Rayleigh Benard convection, which dominates for large inclination angle.

Acknowledgements

The authors wish to acknowledge the continuing support of the Australian Research Council.

References

- [1] Armfield, S. W. and Janssen, R., A direct boundary-layer stability analysis of steady-state cavity convection flow, *Int. J. Heat Fluid Flow*, **17**, 1996, 539–546.
- [2] Armfield, S. W. and Patterson, J. C., Direct simulation of wave interactions in unsteady natural convection in a cavity, *Int. J. Heat Mass Transfer*, **34**, 1991, 929–940.
- [3] Armfield, S. W. and Patterson, J. C., Wave properties of natural-convection boundary layers, *J. Fluid Mech.*, **239**, 1992, 195–211.
- [4] Catton, I., Natural convection in enclosures, *Proc. 6th Int. Heat Transfer Conf.*, 13–43.
- [5] Cianfrini, C., Corcione, C. and Dell’Omo, P. P., Natural convection in tilted square cavities with differentially heated opposite walls, *Int. J. Thermal Sciences*, **44**, 2005, 441–451.
- [6] De Vahl Davis, G., Laminar natural convection in an enclosed rectangular cavity, *Int. J. Heat Mass Transfer*, **11**, 1968, 1675–1693.
- [7] De Vahl Davis, G., Natural convection of air in a square cavity, a benchmark numerical solution, *Int. J. Num. Meth. Fluids*, **3**, 1983, 249–264.
- [8] Hyun, J. M., Unsteady buoyant convection in an enclosure, *Adv. Heat Transfer*, **24**, 1994, 277–320.
- [9] Janssen, R. and Armfield, S. W., Stability properties of the vertical boundary layers in differentially heated cavities, *Int. J. Heat Fluid Flow*, **17**, 1996, 547–556.
- [10] Kuyper, R. A., Van Der Meer, T. H., Hoogendoorn, C. J. and Henkes, R. A. W. M., Numerical study of laminar and turbulent natural convection in an inclined square cavity, *Int. J. Heat Mass Transfer*, **36**, 1998, 2899–2911.
- [11] Mallinson, G. D. and De Vahl Davis, G., Three dimensional natural convection in a box: a numerical study, *J. Fluid Mech.*, **83**, 1977, 1–31.
- [12] Patterson, J. C. and Armfield, S. W., Transient features of natural convection in a cavity, *J. Fluid Mech.*, **219**, 1990, 469–497.
- [13] Patterson, J. C. and Imberger, J., Unsteady natural convection in a rectangular cavity, *J. Fluid Mech.*, **100**, 1980, 65–86.
- [14] Rasoul, J. and Prinos, P., Natural convection in an inclined enclosure, *Int. J. Num. Meth. Heat Fluid Flow*, **7**, 1997, 438–478.